Modeling of Free Surface Flow in a Helical Channel with Finite Pitch

Rigoberto E. M. Morales
rmorales@utfpr.edu.br
Technological University of Paraná – UTFPR
Pos-Graduate Program in Mechanical Engineering and Materials - PPGEM
80230-901 Curitiba, PR, Brazil

Eugênio S. Rosa
Member, ABCM
erosa@fem.unicamp.br
State University of Campinas - UNICAMP
Faculty of Mechanical Engineering
13081-970 Campinas, SP. Brazil

The laminar fully developed free surface flow in a helical channel with finite pitch and rectangular section is modeled. The mass and momentum conservation equations are written in a local orthogonal system and solved numerically using the finite volume method. The free surface position, determined using the height of liquid method, compares favorably against the experimental data. The main and secondary velocity fields are determined as well as the friction factor for Reynolds number ranging from 352 to 856
***Keywords**: free surface flow, helical channel, HOL, finite volume method*

Introduction

Flow in curved ducts occurs in several industrial processes, from heat transfer equipments to turbo-machinery, in chemical reactors to flow separator devices and also in natural phenomena such as river meandering to cite a few. The subject has been drawing attention of the fluid mechanics community for nearly three quarters of a century. Certainly, one of the pioneering works on this subject belongs to Dean (1927). Nowadays the bibliography is extensive. The fluid flow and heat transfer in curved ducts, with or without finite pitches, for different cross-sections have been reviewed by Berger et. al. (1983), Berger (1991), Nandakumar and Masliyah (1986), Shah and Joshi (1987) and Ito (1987).

A curved duct can be described by a local coordinate system whose origin coincides with the curve passing through the duct's cross section center. This curve is characterized by the curvature κ and the torsion τ, to be defined on the next section. For null torsion the curved duct degenerates to a toroidal shape while for null curvature it degenerates in a twisted straight duct. Figure 1 represents, schematically, a curved duct with a square section of size 'a' and pitch $2\pi b$ for increasing values of torsion.

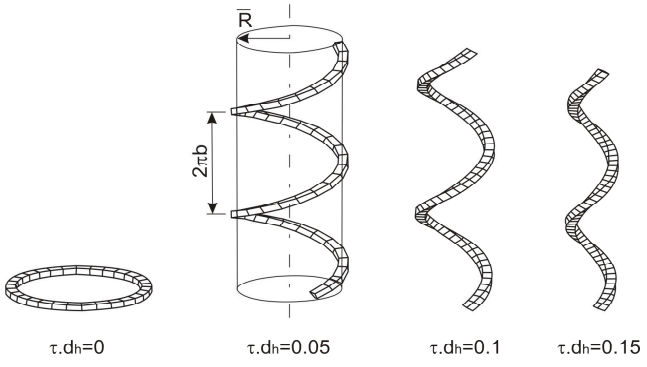

Figure 1. Helical channels with square cross section, constant curvature $\kappa.d_h = 1$ and torsion $\tau.d_h$ spanning from 0 to 0.15.

The main feature in curved ducts is the secondary flow. Near the walls, the fluid is displaced inward due to the centripetal force field induced by the streamline curvature. Considering toroidal ducts in laminar regime the secondary flow is characterized by two counter rotating symmetrical cells. On the other hand for helical ducts, i.e. non-null curvature and torsion, there are two non-symmetrical counter rotating cells which evolve to four when the Reynolds number increases. The non-null torsion present in helical ducts introduces more complexity to the analysis as compared to toroidal ducts. One of the challenging aspects is the description of the governing equations from a coordinate system. The works of Wang (1981) and Germano (1982) addresses the issue of the coordinate system for circular cross section ducts. The former proposes a non-orthogonal coordinate system while the later uses a coordinate transformation to establish an orthogonal coordinate system. The torsion effect on the secondary flow is of first order accordingly to Wang while it is of second order if one employs Germano's coordinate system. Tutle (1990) reconciled the results of Wang and Germano explaining that the differences arouse due to the velocity components calculated by distinct coordinate systems.

The effect of curvature and torsion on the fluid flow and heat transfer in circular cross section pipes have been studied by several authors, among then, Kao (1987), Xie (1990), Hwang and Chao (1991), Liu and Masliyah (1993), Zabielski and Mestel (1998), and Hatzikonstantinou and Sakalis (2004). The works on helical ducts with rectangular cross sections are more recent. Analytical, numerical and experimental works focusing on the critical Reynolds to flow bifurcations, the number of recirculation cells and the increase on the friction factor and heat transfer coefficient in helical ducts with rectangular cross section are found in Bara et al. (1992), Chen and Jan, (1993), Bolinder and Sunden (1995), Bolinder (1996), Thonson et. al. (2001), Sakalis et al. (2005) and Chen et al. (2006).

Despite of the recent efforts towards the flow understanding in helical ducts none of them deals with the flow phenomenon in the presence of a free surface. This subject was motivated by the recent developments on the gas-liquid separators employed by the petroleum industry (Rosa et al. 2001). Free surface helical channel flows are driven the gravity force but the channel's curvature and torsion develop a centrifugal force, tilt the interface and shape the flow velocity field. There is a large body of literature modeling curved free surface channel's flow employing the depth averaged Navier Stokes equations proposed by Rodi (1993), Demuren (1993), Meselhe (2000) and recently, Lu et al. (2004) to cite a few. Albeit this works, none of them deals with the simultaneous effect of curvature and torsion on the flow. The objective of this work is two-fold: propose a simplified orthogonal set of the Navier Stokes equations for helical channels with rectangular cross section and

Paper accepted February, 2007. Technical Editor: Francisco Ricardo Cunha.

solve it for a free surface and fully developed flow employing a height of liquid method to capture the free surface position.

Flow Modeling

The first consideration in flow modeling is the choice of a suitable coordinate system. The helical channel suggests a development from a general curve in space described by $\vec{R}(s)$ coinciding with the channel's axial centerline:

$$\vec{R}(s) = x(s)\vec{i} + y(s)\vec{j} + z(s)\vec{k} \tag{1}$$

where 's' is the arclength along the curve and $\vec{i}, \vec{j}, \vec{k}$ are unit vectors in a fixed Cartesian coordinate system, see Fig. 2. A natural set of orthogonal vectors along 's' is the triad: $\vec{T}(s), \vec{N}(s)$ and $\vec{B}(s)$ corresponding to the tangential, normal and binormal unit vectors. They are related to the curvature, κ, and to the torsion, τ, by the Frenet relationship (Hsu, 1969):

$$\vec{T}(s) = \frac{d\vec{R}}{ds}, \quad \vec{N}(s) = \frac{1}{\kappa}\frac{d\vec{T}}{ds}, \quad \vec{B}(s) = \vec{T}\times\vec{N},$$
$$\frac{d\vec{N}}{ds} = -\kappa\vec{T} + \tau\vec{B}, \quad \frac{d\vec{B}}{ds} = -\tau\vec{N}. \tag{2}$$

The present analysis applies to helical channels with fixed diameter and pitch; i.e., channels with constant curvature and torsion. For an observer moving along s, $\vec{T}$ is invariant but $\vec{N}$ and $\vec{B}$ are rotating. The geometrical properties κ, τ and the angle with the horizontal, α, are defined in terms of the helix's radius $\overline{R}$ and helix's pitch $2\pi b$ accordingly:

$$\kappa = \frac{\overline{R}}{\overline{R}^2 + b^2}; \quad \tau = -\frac{b}{\overline{R}^2 + b^2}; \quad \alpha = \arctan\left(b/\overline{R}\right) = \arctan\left(-\tau/\kappa\right). \tag{3}$$

Also the helix arclength 's' and the displacement angle φ, measured counter-clockwise, are related by:

$$\varphi(s) = \frac{s - s_0}{\sqrt{\overline{R}^2 + b^2}}. \tag{4}$$

One natural choice for coordinate is the (s, x', y') system where s is the arclength of the channel's centerline which is always parallel to the vector $\vec{T}$ and the x' and y' which lies in a plane orthogonal to the vector $\vec{T}$. The vector position $\vec{r}$ in terms of (s, x', y') is:

$$\vec{r} = \vec{R}(s) + x'\vec{i}' + y'\vec{j}'. \tag{5}$$

where $\vec{i}'$ and $\vec{j}'$ rotate with respect to $\vec{N}$ and $\vec{B}$ as one proceeds along 's' in such a way to undo the torsional effect, see Fig. 2. Germano (1982) recognized that the plane (x'y') has an arbitrary origin, ϕ_0 and proposed a compensation angle $\phi(s)$ to the torsional effect such that:

$$\phi(s) = \int_{s_0}^{s} \tau ds' + \phi_0. \tag{6}$$

Equation (6) is known as Germano's transformation. The representation of the (x,y,z) and (x',y',s) coordinates as well as the rotating angle $\phi(s)$ are shown in Fig. 2.

The metric of the (s, x', y') coordinate system arises from the scalar product of the infinitesimal changes of the position vector $\vec{r}$ and from the use of the Frenet relationships:

$$d\vec{r}\cdot d\vec{r} = \left[1 - \kappa\left(x'\cos(\phi(s)+\phi_0) - y'\sin(\phi(s)+\phi_0)\right)\right]^2 ds^2 + dx'^2 + dy'^2 \tag{7}$$

The lack of cross products among the infinitesimal displacements in Eq. (7) reveals that the (s,x',y') coordinate system is orthogonal. For the sake of convenience, but without loss of generality, it is considered that $\phi_0 = s_0 = 0$ so the scale factors, for each orthogonal direction become:

$$h_{x'}^2 = 1, \quad h_{y'}^2 = 1 \quad \text{e} \quad h_s^2 = \left[1 - \kappa x'\cdot\sin(\tau\cdot s) + \kappa y'\cdot\cos(\tau\cdot s)\right]^2 \tag{8}$$

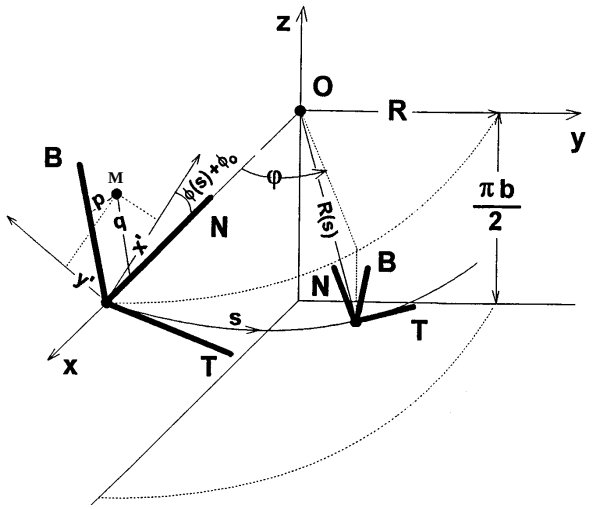

Figure 2. Schematic representation of the axial center line, s, the Frenet triad and the rotating coordinate system (s,x',y') resulting from Germano's transformation.

Tutle (1990) refers to this coordinate system as space-centered. Constant values of 's' define an (x',y') plane which is orthogonal to the axial flow direction. Due to the x' and y' rotation, the channel boundaries are not constant but 's' dependent. The successive cross sections of the helical channel are mapped on the (s,x',y') system as a twisted channel with an angle α with the horizontal, see schematic representation in Fig. 3a and 3b. The necessary channel's length to rotate the cross section of $\pi/4$ radians is $(\pi/4).(1/\tau)$ as indicated on Fig. 3b.

The usefulness of Germano's transformation lies on the compact representation of the transport equations due to the orthogonally of the coordinate system. On the other hand it brings one disadvantage for rectangular cross section ducts, the boundary is not invariant but it continuously changes along 's' as suggested by Fig. 3b. To overcome this difficult one has to take two approximations. The first deals with the area transformation between coordinate. The relationship of the element of area between the physical and transformed planes is approximated by:

$$dx'\cdot dy' \cong (dx\cdot dy)\cdot\cos(\alpha) \tag{9}$$

Equation (9) approximate the cross section area on the (x',y') plane to the physical helical channel cross section area projected by the channel's centerline inclination angle, α. This procedure is exact

for toroidal channels but the bias increases with the increase of the torsion. Alves (2000) found a maximum deviation between areas of 2% for a series of helical channels with distinct aspect ratio, curvature and torsion. The second approximation deals with the twist rate. A direct comparison between the necessary length 's' to rotate the cross section by 2π and the hydraulic diameter of the section, d_h, gives an estimate of how fast the twist angle changes. When the ratio $2\pi/(\tau.d_h) >> 1$ the channel has a slow twist rate, the flow changes slowly along 's' direction in such a way that is reasonable to assume fully developed flow, i.e., $\partial/\partial s = 0$. Since the flow is considered invariant along 's' and centering the analysis in cross sections where $s = (2\pi/\tau).n$ (n=1, 2, 3,…) the scale factors take the form,

$$h_s = 1 + \kappa y' , \quad h_{x'} = h_{y'} = 1.0 , \tag{10}$$

with the first and second order derivatives given by:

$$\frac{\partial h_s}{\partial x'} = 0 ; \ \frac{\partial h_s}{\partial y'} = \kappa ; \ \frac{\partial h_s}{\partial s} = -x'\tau\kappa ; \quad \frac{\partial}{\partial s}\left(\frac{\partial h_s}{\partial x'}\right) = -\tau\kappa ; \quad \frac{\partial}{\partial s}\left(\frac{\partial h_s}{\partial y'}\right) = 0 \tag{11}$$

The form of the transport equations for a generic variable ϑ in fully developed flow is:

$$\frac{\partial(\rho\vartheta)}{\partial t} + \frac{1}{h_{x'}.h_{y'}.h_s}\left[\frac{\partial}{\partial x'}\left(h_{y'}.h_s J^{\vartheta}_{x'}\right) + \frac{\partial}{\partial y'}\left(h_{x'}.h_s J^{\vartheta}_{y'}\right)\right] = S^{\vartheta} + P^{\vartheta} , \tag{12}$$

where S^{ϑ} are the source terms, J^{ϑ}_j and P^{ϑ} represent the transport tensor and the pressure terms,

$$J^{\vartheta}_j = \rho V_j \vartheta - \frac{\Gamma}{h_j}\frac{\partial \vartheta}{\partial x_j} \quad \text{and} \quad P^{\vartheta} = -\frac{1}{h_j}\frac{\partial P}{\partial x_j}, \tag{13}$$

and Γ is the diffusion coefficient.

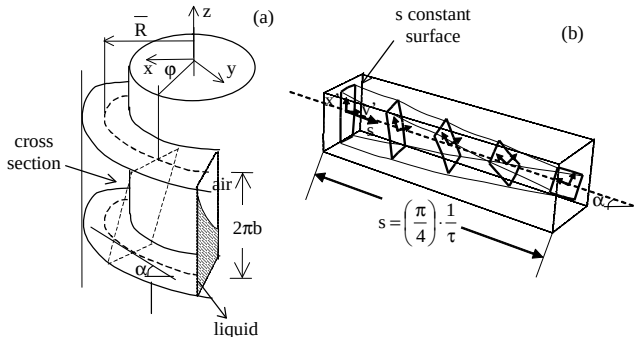

Figure 3. Schematic representation of the helical channel (a) physical plane or (x,y,z) coordinates, (b) transformed plane or (x',y', s) coordinates.

The mass conservation equation is set up substituting ϑ =1, Γ = S^{ϑ} = P^{ϑ} = 0 as well as formulae from Eqs. (10) and (11) into Eq. (12). Similarly the momentum transport equations are set by choosing ϑ = w or u or v which represent the flow velocities along the s, x' and y' directions, respectively. The diffusion coefficient is the dynamic liquid viscosity, $\Gamma = \mu$. Source terms arise from transport tensor due to the products of the derivatives of the scale factors. Finally the pressure term exists only on the x'y' plane due to the secondary flow currents. There is no pressure gradient along the 's' direction since this is a fully developed gravity driven flow. Table 1 summarizes the substitutions for the mass and momentum equations.

For toroidal channels, i.e. null torsion, the source terms of the transport equations reduces to those presented by Ghia and Sokhey (1977). But for helical channels the influence of non-null torsion appears on the momentum equation as source terms resulting from products of other variables with the helix torsion, see Table 1 for reference.

Numerical Method

The fully developed flow equations in conjunction with the interface tracking method are embodied in the numerical code. This section briefs the particular features of the fully developed flow and of the interface tracking models. It also depicts the solution algorithm, the boundary and initial condition and, at last, presents a grid test.

Usually fully developed flows are achieved numerically using forward-marching procedures from the inlet plane to successive planes in the main flow direction until the flow properties are invariant along the axial direction. Clearly, this procedure is inefficient if one recognizes that in fully-developed flows the axial convection and the diffusion are null. So, if the mass flow or the mean axial pressure gradient are specified, the solution may be obtained by performing calculations repeatedly in a two dimensional grid along the (x',y') plane. A detailed description of the two-dimensional grid has been provided by Madhav (1992), but in essence the method calculates the axial pressure gradient iteratively from overall continuity by means of a truncated form of the streamwise momentum equation.

The fully developed free surface flow has two distinguished features related to the axial momentum equation: it is driven by the gravity and it has no pressure gradient. The w velocity is treated as a scalar once it has no coupling with the pressure terms and, for any given grid node, w may change value on (x',y') but it is invariant along 's' direction. The secondary flow is determined solving the u and v momentum equations coupled with the lateral pressure gradients, $-\partial p/\partial x'$, $-\partial p/\partial y'$. The mass conservation equation reduces to u and v components but it has an artificial mass source term due to the difference between the given axial mass flow rate and the resulting axial mass flow rate, $\dot{M}_r$, the last one calculated from the w velocity field. The mass source term is defined as:

$$S_M = \dot{M}_g - \dot{M}_r . \tag{14}$$

When the resulting mass flow rate is equal to the given mass flow rate the mass source vanishes and the w velocity field is converged.

Table 1. Terms of transport equations applied to fully developed flow.

ϑ	$J^{\vartheta}_{x'}$	$J^{\vartheta}_{y'}$	S^{ϑ}	P^{ϑ}
1	ρu	ρv	0	0
u	$\rho uu - \mu\frac{\partial u}{\partial x'}$	$\rho vu - \mu\frac{\partial u}{\partial y'}$	$\frac{\mu}{h_s^2}.\tau.\kappa.w - \rho g \cdot Cos\alpha$	$-\frac{\partial P}{\partial x'}$
v	$\rho uv - \mu\frac{\partial v}{\partial x'}$	$\rho vv - \mu\frac{\partial v}{\partial y'}$	$\frac{\rho\kappa w^2}{h_s} - \mu\frac{\tau\kappa^2}{h_s^3}x'w - \mu\left[\frac{\kappa}{h_s}\right]^2 v$	$-\frac{\partial P}{\partial y'}$
w	$\rho uw - \mu\frac{\partial w}{\partial x'}$	$\rho vw - \mu\frac{\partial w}{\partial y'}$	$-\frac{\rho\kappa vw}{h_s} - \mu\frac{\tau\kappa}{h_s^2}u + \mu\frac{\tau\kappa^2}{h_s^3}x'v - \mu\left[\frac{\kappa}{h_s}\right]^2 w + \rho g \cdot Sin\alpha$	0

The free interface is captured using a height function method which was originally proposed by Nichols and Hirt (1973). They extended the idea of interface marker particles by relating interface points to points to a certain reference plane. The interface location is then defined by its height or distance from the reference plane. The major limitation is that it applies only to a single interface for each vertical column of cells, i.e., it does not handle multiples interfaces neither interface overturn. On the other hand it has the advantage of tracking the interface using the mass conservation equation rather than obeying a kinematic condition. The method, henceforth denominated by height of liquid – HOL, is purely algebraic, does not exhibit numerical diffusion, is extremely efficient in terms of computer storage and is most suitable for modeling of non-complex free surfaces (Spalding, 1994; Mashayek and Ashgriz, 1994).

The relative importance of the surface tension on the model is accessed by the Bond number. Experimental evidences show that the interface is smooth and exhibits a curvature of the order of the channel's hydraulic diameter. The ratio between the gravity and surface tension forces, $\rho g d_h^2 / \sigma$, gives Bo of 160 meaning a surface tension force two orders of magnitude less than the gravity force. Based on this estimate the effect of surface tension was neglected on the HOL method.

This study employs a helical channel, with dimensions defined in Table 3, for which experimental data is available. The transport equations are discretized employing the finite volume method (Patankar, 1980) with a staggered grid and a hybrid scheme for the convective terms. The initial condition is a flat horizontal interface with w, u and v velocities initially set to 10^{-10}. The no-slip conditions are prescribed at the walls. At the interface the velocity, the shear and the normal stresses are intrinsically satisfied by the HOL method, as it treats the two fluids as single phase with step changes on the fluid properties defined by the interface position. A false transient method is used to advance the numerical solution with a constant time step of 0.005 second. At each time step the momentum and mass equations are solved for velocities and pressure, a new interface positioning is determined by the HOL method and the mass source, Eq. (14), is evaluated. The fully developed flow is achieved when the source of mass is less than 0.0001. The computational procedure was set up within Phoenics-CFD 2.0 software package and it is fully described in Morales (2000).

A grid test was conducted to access the solution sensitivity on the grid size. The test employed three grids: two uniform grids with 2400 and 1375 volumes and one non-uniform grid with 1375 volumes with a finer mesh near the walls. The reference value to the grid test was the averaged friction factor, $\overline{f_b}$, as defined by Eq. (20). The test results are reported in Table 2. The uniform grid is not so sensitive on the mesh size and exhibits a deviation on $\overline{f_b}$ on 3%. But the non-uniform grid, with the same 1375 volumes, has a 1.5% deviation. The non-uniform grid is preferred for demanding less computational effort without worsening the $\overline{f_b}$ estimate.

Table 2. Grid test.

Grid (x',y')	Type	Number of Volumes	Grid Aspect Ratio	$\overline{f_b}$
80x30	Uniform	2400	1.8	0.065
55x25	Uniform	1375	2.1	0.063
55x25	Non-uniform	1375	not apply	0.064

Experimental Data

The interface position was experimentally determined for a helical channel with size described in Table 3. The pitch is 114.9 mm while the centerline radius $\overline{R}$ is 56.6 mm. The channel curvature and torsion are shown in the fourth and fifth columns. The centerline angle with horizontal, α, is of 17.95 degrees. The channel' height, width and cross section area, H, d and A_t, as seen on plane x'y', are in the seventh to ninth columns. Finally the last column shows the channel hydraulic radius defined as the ratio between the cross section area A_t and the channel perimeter, 2(H+d). A schematic view of the channel's cross section on x'y' and xy plane is shown in Figure 4 to aid the understanding.

The experimental measurements were taken at the helix section after five complete turns, or φ = 1800 degrees, downstream the channel inlet to assure a fully developed flow. The gas and liquid phases were air and a solution of corn syrup and water at concentrations of 82% in volume exhibiting Newtonian behavior. The density and viscosity of the liquid phase were of 1324 kg/m^3 and 96 cP, respectively. The free surface position was measured for a set of three runs with mass flow rates of 0.55 kg/s, 0.98 kg/s and 1.57 kg/s. The observed flow regime in all runs was laminar. The fluid properties and the flow rates for runs #1 to #3 are in Table 4.

Table 3. Channel's main dimensions.

$2\pi b$ (mm)	$\bar{R}$ (mm)	κ (1/m)	τ (1/m)	α (degree)	H (mm)	d (mm)	A_t (mm^2)	R_{HC} (mm)
114.9	56.5	16.04	5.19	17.95	109.28	24.10	2633.6	9.87

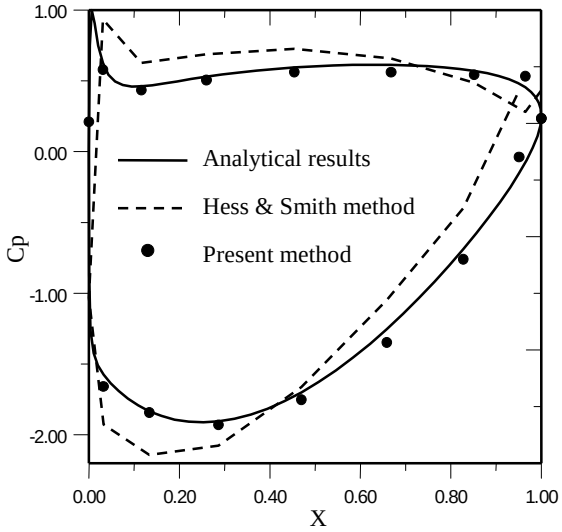

Figure 4 . Channel's cross section and nomenclature for the x'y' and xy plane.

Table 4. Tests flow rates and fluid properties.

Test #	Mass flow rate (kg/s)	Density (kg/m^3)	Viscosity (cP)	Liquid Solution
1	0.55	1324.0	94.50	Syrup 82%
2	0.98	1324.0	96.70	Syrup 82%
3	1.57	1324.0	98.96	Syrup 82%

The experimentally determined free surface position is shown in Figs 5 as a scatter plot. The experimental technique employed a parallel wire probe with a traverse mechanism to displace the probe. The experimental data consist of liquid film heights taken along radial positions having as reference the bottom of the channel. The uncertainty of the liquid height is up to 4 mm which, in terms of error bars, is equivalent to two minor ticks on the y scale of Fig. 5. The uncertainties result from the probe positioning, probe calibration procedure, changes in liquid electrical conductivity due to the ambient temperature variation and to the corn syrup concentration. The experimental set up and the measurement technique are described in Alves (2000). The data analysis is presented in the next section in conjunction with the numerical results.

Results

Figure 5 compares the numerical estimates of the interface position against the experimental data for tests #1 to #3. The experimental data display the interface climbing the outer wall due to the centrifugal force induced by the streamline curvature. The numerical estimates of the interface's position follow the same trend within 2mm bias. The data agreement, bounded by the experimental uncertainty, gives support to the physical and numerical consistencies of the model.

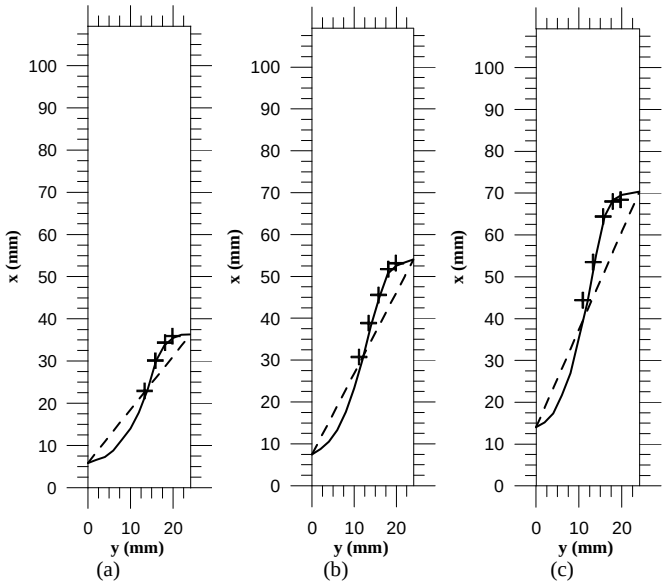

Figure 5. Interface position : (a) Re = 353 & Fr = 1.15, (b) Re = 484 & Fr = 1.67 and (c) Re = 602 & Fr = 2.20. (___) numerical, (+++) experimental (Alves, 2000), (- - -) mean interface tilt angle.

Knowing the interface position it is possible to determine the channel-flow properties listed in Table 5. The liquid holdup, ε, is defined as the ratio between the cross section area occupied by the liquid, A_l, and the channel cross section area, A_t. The liquid wetted perimeter, P_m, is determined summing the wall lengths wetted by the liquid. The mean axial velocity, w_m, the hydraulic radius, R_H, and the Reynolds and Froude channel's numbers are:

$$w_m = \frac{\dot{M}_{in}}{\rho \cdot A_t \cdot \varepsilon}, \qquad R_H = \frac{A_t \cdot \varepsilon}{P_m}; \qquad Re = \frac{4 \cdot \rho \cdot w_m \cdot R_H}{\mu}; \quad Fr = \frac{\kappa \cdot w_m^2}{g}, \tag{15}$$

where ρ and μ refer to the liquid density and viscosity respectively.

As seen from Table 5, all listed channel-flow properties increases as the mass flow rate increases. One of the relevant variables to channel's design is the liquid holdup. Liquid holdup of unit defines, in terms of mass flow rate, the channel's maximum capacity. The tests #1 to #3 disclose a steady increase on the liquid holdup from 18.7% to 76.9% when the mass flow rate changed from 0.55 kg/s to 1.57 kg/s. Complementary, while the mass flow rate increased by a factor of 2.8 cross section area taken by the liquid increased by a factor of 4.1 and the liquid mean velocity by a factor of 1.4. Therefore the channel's mass flow rate is mostly increased by the increase on the liquid holdup rather than by the increase on the liquid mean velocity.

Table 5. Channel flow properties.

Test #	Mass (kg/s)	ε (%)	w_m (m/s)	P_m (mm)	R_H (mm)	Re	Fr
1	0.55	18.7	0.84	66.0	7.47	352.8	1.15
2	0.98	27.7	1.01	83.8	8.71	483.9	1.67
3	1.57	76.9	1.16	105.5	9.72	601.6	2.20

The free surface is displaced outwardly due to the combined action of the gravity and centrifugal force fields. The averaged interface's tilt angle with the horizontal is estimated taking the arc tangent of the Froude number. For tests #1 to #3 these values are, respectively, of 49, 59 and 66 degrees which closely represent the averaged tendency of the numerical data, see dashed lines in Fig. 5.

The axial velocity field and the secondary flow vector plot are shown in Fig. 6. The maximum axial velocity happens near the air-liquid interface but shifted outwardly due to the centrifugal force action on the liquid body. From a qualitative point of view this is a distinguished feature as compared with open channel flows without curvature. Close to the interface the gradient of the axial velocity is normal to the interface due to the viscosity difference between the liquid and the air. The curves of constant axial velocity nearly follow the channel's boundaries but, surprisingly enough, they show a local maximum located at the midpoint nearly above the bottom wall. This low shear region also coincides with the center of the main secondary flow cell. The same feature is also found for flows in closed helical ducts, Bolinder and Sunden (1995). Figure 6 shows the secondary currents exhibiting two non-symmetrical counter rotating recirculation cells. The cells are one on top of the other. The lower one covers a greater area as compared with the upper one. The clockwise direction of the lower cell is due the action of the pressure gradient on the liquid near the lower wall which, being retarded due to the viscous forces, do not have enough inertia to counter-balance the pressure gradient and is driven inward. The upper cell, driven by the lower cell, rotates counter-clockwise.

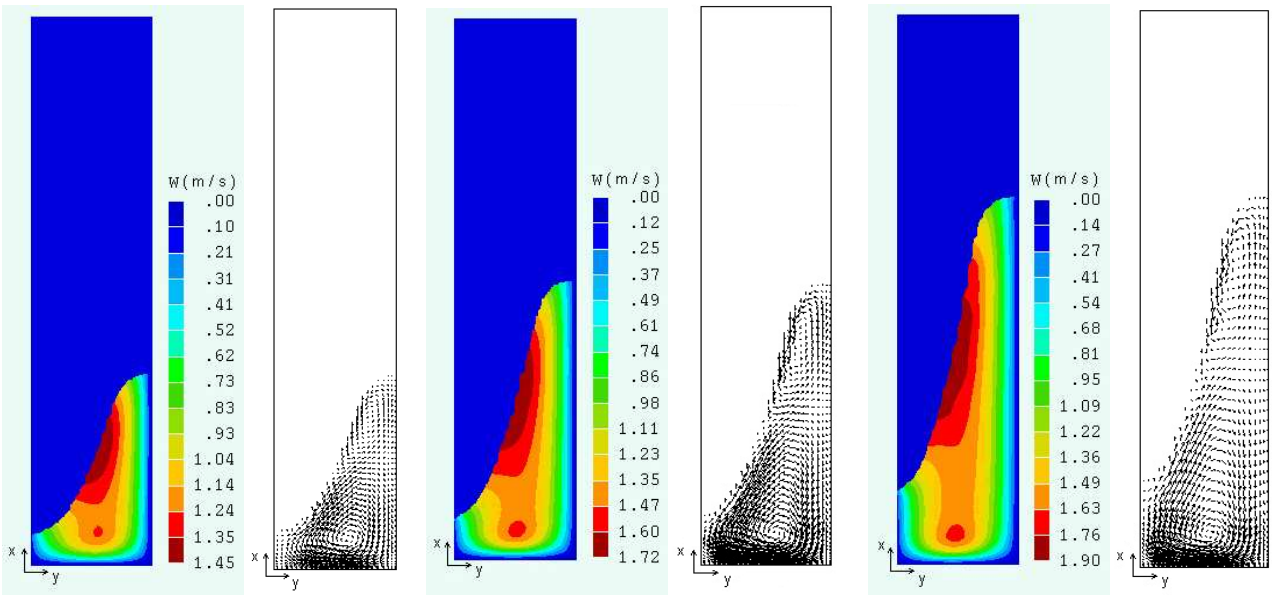

(a) (b) (c)

Figure 6. Axial velocity field and secondary flow field; (a) Re = 353 & Fr = 1.15, (b) Re = 484 & Fr = 1.67 and (c) Re = 602 & Fr = 2.20.

The secondary current affects substantially the channel friction factor. The local wall shear stress is evaluated numerically by:

$$\tau_w = \mu \frac{\sqrt{w_w^2 + v_w^2}}{\delta}, \tag{16}$$

where δ is the distance to the wall of the first grid node adjacent to the wall and w_w and v_w are, respectively, the axial and the secondary velocities of the first node adjacent to the walls. The local wall shear is conveniently expressed as a local friction factor f by Eq. (17):

$$f = \frac{\tau_w}{0.5 \cdot \rho_L w_m^2}. \tag{17}$$

The local friction factor along each channel's walls is in Fig. 7. For referencing purposes the figure inset identifies the channel's walls. The local friction factor exhibits two general characteristics: null at the channel's corners and inversely proportional to the Reynolds number. The local friction factor for the *inner wall* is null at the corner and then increases as the distance from the inner corner increases up to a x distance about 12 mm because this is roughly the maximum wetted extension along inner wall, see Fig. 5. The friction factor's growing rate does not change substantially when the

Reynolds almost doubles from 353 to 601. At the *outer wall* the friction factor has a fast growing rate at positions away from the corner. At distances greater than 8 mm from the corner it achieves an almost constant value. Further out from the corner it then exhibits a falling tendency as the liquid-air interface is approached. Finally the local friction factor at the *lower wall* has a minimum near the corner regions, y<1mm and y>23mm and a maximum near the mid distance coinciding with the lower secondary cell center.

The mean friction factor, $\overline{f_m}$, is defined by weight-average procedure of the local friction factor along the wetted perimeter:

$$\overline{f_m} = \frac{1}{P_m} \int_0^{P_m} f \cdot d\ell \,. \tag{18}$$

Equation (18) requires detailed information regarding the velocity field and the wall distance to compute the local friction factor. There is though a less troublesome way to evaluate the mean friction factor. Since the fully developed flow is inertia free the mean shear force is balanced by the liquid weight:

$$\overline{\tau_w} \cdot P_m = \rho \cdot g \cdot \mathrm{Sin}\alpha \cdot \varepsilon \cdot A_t \,, \tag{19}$$

where $\overline{\tau_w}$ represents the mean shear stress acting on the channel's wetted perimeter. From Eq. (19) is possible to express $\overline{\tau_w}$ in terms of mean friction factor, $\overline{f_b}$, which turns to be:

$$\overline{f_b} = \frac{2 \cdot \varepsilon \cdot A_t \cdot g \cdot \mathrm{Sin}(\alpha)}{P_m \cdot w_m^2} \,. \tag{20}$$

Equation (20) is readily evaluated employing the averaged channel-flow properties given in Table 5. A straightforward comparison between the procedures stated by Eq. (18) and (20) exhibits a maximum deviation of 1% as shown in Table 6. The satisfactory agreement between the two procedures reassures the model consistency because the same averaged friction factor is achieved using two distinct procedures: one based on local flow field information while the other supported by averaged flow properties.

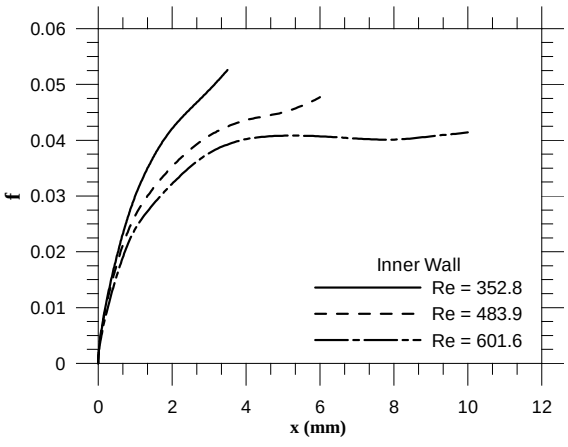

Figure 7. Local wall friction factor along the inner, outer and lower walls for tests #1, #2 and #3.

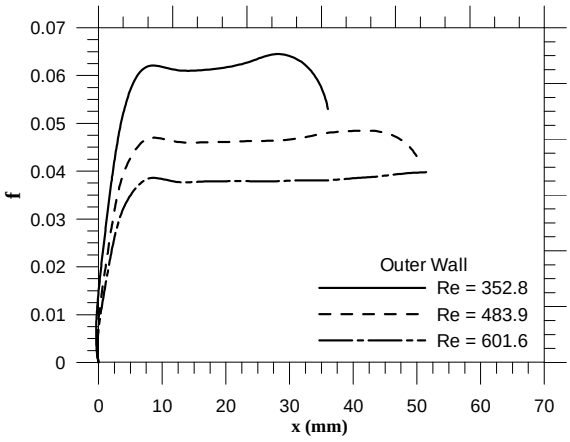

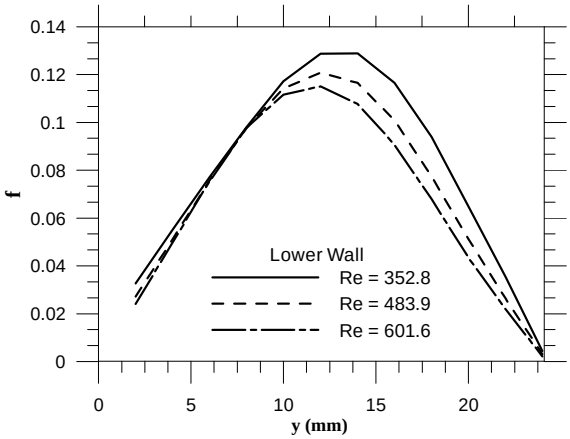

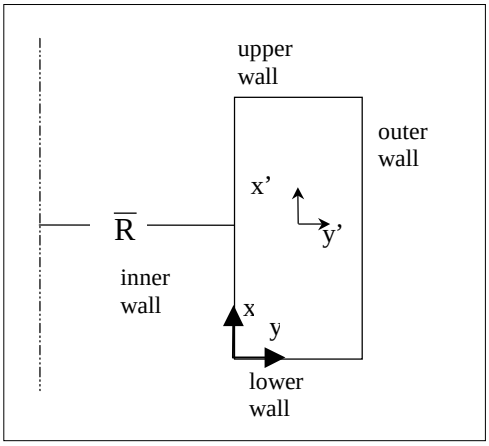

Figure 7. (Continued)..

Table 6. Friction factors.

Test #	Re	$\overline{f_m}$	$\overline{f_b}$	$\frac{\overline{f_m}-\overline{f_b}}{\overline{f_b}}$ x100
1	352.8	0.0628	0.0635	-1.0
2	483.9	0.0506	0.0511	-1.0
3	601.6	0.0439	0.0438	+0.2

Despite of the small deviation between $\overline{f_m}$ and $\overline{f_b}$ the later is preferred because it comes from averaged flow properties which are less prone to oscillations than first order derivatives which are the basis to evaluate $\overline{f_m}$.

The friction factor augmentation due to curvature and torsion effects is assessed comparing $\overline{f_b}$ against the friction factor occurring in a laminar, fully developed straight channel flow with square cross section, fs = 14.22/Re (White 1986). A series of 16 runs with distinct mass flow rates was conducted to render numerical values of $\overline{f_b}/f_S$. The results, shown in Fig. 8, exhibit the ratio $\overline{f_b}/f_S$ growing monotonically with Re. Furthermore, the effect of curvature and torsion enhances the friction factor by a factor of 1.3 for Reynolds number as low as 200 and attain factor of 2.3 for Reynolds number of 1200.

The friction factor ratio is also compared against the Bolinder (1995) correlation for forced flow in helical pipe. This correlation resulted from numerical laminar flow simulations in a closed helical channel employing a non-orthogonal coordinate system. It holds for $4\kappa R_H < 0.4$ and $Re < 600$ with the definitions of R_H and Re given in Eq. (15). Even though Bolinder's correlation does not account for the asymmetries due to the outward displacement of the free surface, the results matches the present work estimates within 5%. This evidence supports once more the reliability of the physical and numerical models developed.

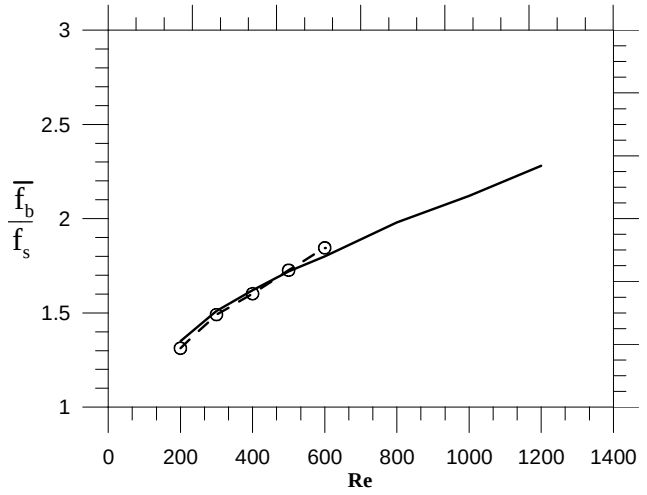

Figure 8. Friction factor ratio against Re (—) present work, (-- o- -) Bolinder (1995).

Conclusion

A numerical model is developed to simulate the fully developed flow in laminar regime occurring in a helical channel with a free surface. The transport equations are written for an orthogonal coordinate system using Germano's (1982) transformation. The cross sections of the helical channel are mapped into successive cross sections of a twisted channel with the same angle with the horizontal. To enforce the fully developed condition the twist angle has to change slowly with the axial position or $2\pi/(\tau d_H) >> 1$. The interface position was numerically determined employing a height method based on mass conservation for interface capture. The transport equation set was solved using the finite volume method for a single slab of cells. The consistencies of the physical modeling and of the numerical procedures are favorably checked against experimental data of the free surface position and by the averaged friction factor estimates.

The numerical data disclosed the free surface's position the axial velocity field, the secondary flow currents and the friction factor. The channel's flow capacity is directly associated with the liquid holdup, i.e., an increase on the flow rate would increase the liquid holdup. The centrifugal force field displaces the body of liquid, within the channel's cross section, outwardly. The free surface's tilt angle increases as the channel's Froude increase and, for the present tests, its averaged value ranged from 49 to 66 degrees with the horizontal. The axial velocity field has a maximum at the free surface but shifted outwardly due to the centrifugal field. Close to the interface the axial velocity gradient is normal to the interface due to the viscosity difference between the liquid and the air. The secondary flow has two recirculation cells. The channel's curvature and torsion have a strong effect on the averaged friction factor. For Reynolds spanning from 200 up to 1200 the averaged friction factor is of 1.3 to 2.3 times greater than the friction factor found in an equivalent straight channel.

Acknowledgments:

The authors wish to thank to the reviewers of the JBSMSE for the raised points which enhanced this work's quality, also Rigoberto E. M. Morales would like to thanks to CAPES for his doctoral scholarship.

References

Alves, L. G., 2000, "Free surface flow in helical channel: interface and friction factor determination", M. Sc. Thesis (in Portuguese), Faculdade de Engenharia Mecânica, Universidade Estadual de Campinas, Campinas, SP, Brazil.

Bara, K., Nandakumar, K. and Masliyah, J. H, 1992, "An experimental and numerical study of the dean problem: flow development towards two-dimensional multiple solutions", *J. Fluid Mechanics*, Vol. 244, pp. 339-376,.

Berger, S. A., Talbot, L. and Yao, L. S.,1983, "Flow in curved ducts", *Ann. Rev. Fluid Mechanics*, Vol. 15, pp. 461-512.

Berger, S.A., 1991, "Flow and heat transfer in curved pipes and tubes", *AIAA Paper*, 91-0030.

Bolinder, C. J., 1995, "The effect of torsion on the bifurcation structure of laminar flow in a helical square duct," *Journal of Fluids Engineering*, Vol. 117, pp. 242-248.

Bolinder, C. J., 1996, "First-and higher-order effects of curvature and torsion on the flow in a rectangular duct", *J. Fluid Mechanics*, Vol.314, pp. 113-138.

Bolinder, C. J. e Sunden, B., 1995, "Flow visualization and LDV measurements of laminar flow in a helical square duct with finite pitch", *Experimental Thermal and Fluid Science*, Vol. 11, pp. 348-363.

Chen, W. H. e Jan, R., 1993, "The torsion effect on fully developed laminar flow in helical square ducts", *Journal of Fluids Engineering*, Vol. 115, pp. 292-301.

Chen, Y., Chen, H., Zhang, B. and Hsieh, H.T., 2006, "Fluid flow and convective heat transfer in a rotating helical square duct", *Int. J. Thermal Sci.*, Vol. 45, pp. 1008-1020.

Dean, W. R., 1927, "Note on the motion of fluid in a curved pipe", *Phil. Mag*., Vol. 4, pp. 208-223.

Demuren, A.O., 1993, "A numerical model for flow in meandering channels with natural bed topography", *Water Resour. Res*., Vol. 29, No. 4, pp. 1269-1277.

Germano, M., 1982, "On the effect of torsion on a helical pipe flow", *J. Fluid Mechanics*, Vol. 125, pp. 1-8.

Ghia, K. N. and Sokhey, J. S., 1977, "Laminar incompressible viscous flow in curved ducts of regular cross-sections", *Journal of Fluids Engineering*, Vol. 99, pp. 640-648.

Hatzikonstantinou P.M. and Sakalis, V.D., 2004, "A numerical-variational procedure for a laminar flow in curved ducts", *Int. J. Numer. Methods Fluids*, Vol. 45, pp.1269-1289.

Hsu, Hwei P., "Vector Analysis", 1969, Simon and Schuster.

Hwang G.J. and Chao, C.H., 1991, "Forced laminar convection in a curved isothermal duct", *ASME J. Heat Transfer*, Vol. 113, pp. 48-56.

Ito, H., 1987, "Flow in curved pipe" *Japan Soc. Mech. Engng. Int. J.*, Vol. 30, pp. 543-552.

Kao, H.C., 1987, "Torsioin effect on fully developed flow in a helical pipe", *J. Fluid Mech*., Vol. 184, pp. 335-356.

Liu, S. and Masliyah, J.H., 1993, "Axilally invariant laminar flow in helical pipes with finite pitch", *J. Fluid Mech*., Vol. 251, pp. 315-353.

Lu, W.Z., Zhang, W.S., Cui, C.Z., Leung, A.Y.T., 2004, "A numerical analysis of the free surface flow in curved open channel with velocity-pressure-free-surface correction", *Computational Mechanics*, Vol. 33, pp. 215-233.

Madhav, M. T., 1992, "A numerical algorithm for the simulation of fully-developed flows", Msc. Thesis, University of Greenwich, UK.

Mashayek, F. and Ashgriz, N. "A height-flux method for simulating free surface flows and interfaces", *Int. J. Numer. Methods en Fluids*, Vol. 17, pp. 1035-1054, 1993.

Meselhe, E.A., 2000, "Three-dimensional numerical model for open channels with free-surface variations", *J. Hydr. Res*., Vol. 38, No. 2, pp. 15-121.

Morales, R. E. M., 2000, "Numeric simulation of the free surface flow in an helical channel of rectangular cross section", D. Sc. Thesis (in Portuguese), Faculdade de Engenharia Mecânica, Universidade Estadual de Campinas, Campinas, SP, Brazil.

Nandakumar, K. Masiyah, J.H., 1986, "Swirling flow and heat transfer in coiled and twisted pipe", *Adv. Transport Processes*, Vol. 4, pp. 49-112.

Nichols, B. D. and Hirt, C. W., 1973, "Calculating three-dimensional free surface flows in the vicinity of submerged and exposed structures", *J. Comp. Physics*, Vol. 12, pp. 234-246.

Patankar, S.V., 1980, "Numerical Heat Transfer and Fluid Flow", Hemisphere.

Rodi, W., 1993, "Turbulence Models and Their Application in Hydraulics", IAHR , 3rd ed.

Rosa, E. S., França, F. A. and Ribeiro, G. S., 2001, "The cyclone gas-liquid separator: operation and mechanistic modeling", *J. Petroleum Sci. and Engng*. , Vol 32, 2-4, pp. 87-101.

Sakalis, V.D., Hatxikonstantinou, P.M. and Papadopoulos, P.K., 2005, "Numerical procedure for the laminar developed flow in a helical square duct", *J. Fluids Engineering*, Vol. 125, pp. 136-148.

Shah, R. K and Joshi, S. D., 1987, "Convective heat transfer in a curved duct", Handbook of Single-Phase Convective Heat Transfer, John Wiley, NY.

Spalding, D. B., 1994, "The PHOENICS Encyclopedia", CHAM Ltda., London, UK.

Thonson, D.L., Bayazitoglu, Y. and Meade Jr, A.J., 2001, "Series solution of low dean and germano number flows in helical rectangular ducts", *Int. J. Therm. Sci*, Vol. 40, pp. 937-948.

Tutle, E. R., 1990, "Laminar flow in twisted pipes", *J. Fluid Mechanics*, Vol. 219, pp. 545-570.

Wang, C. Y., 1981, "On the low-Reynolds-number flow in a helical pipe", *J. Fluid Mechanics*, Vol. 108, pp. 185-194.

White, F.M., 1986, "Fluid Mechanics", Mc Graw Hill, 2nd edition.

Xie, D.E., 1990, "Torsion effect on secondary flow in a helical pipe", *Int. J. Heat Mass Transfer*, Vol. 11, pp. 114-119.

Zabielski, L. and Mestel, A.J., 1998, "Steady flow in a helically symmetric pipe", *J. Fluid Mech*., Vol. 370, pp. 297-320.